RSC Advances

ROYAL SOCIETY OF CHEMISTRY

www.rsc.org/advances

Table of Content

Stable and reversible doping of graphene by using KNO_3 solution and photo-desorption current response

M. Farooq Khan, M. Zahir Iqbal, M. Waqas Iqbal, Volodymyr M. Iermolenko, H. M. Waseem Khalil, Jungtae Nam, Keun Soo Kim, Hwayong Noh and Jonghwa Eom*

Department of Physics and Graphene Research Institute, Sejong University, Seoul 143-747, Korea

We found stable n-type doping and carrier mobility improvement of graphene by using KNO_3 solution and investigated photo-desorption current response.

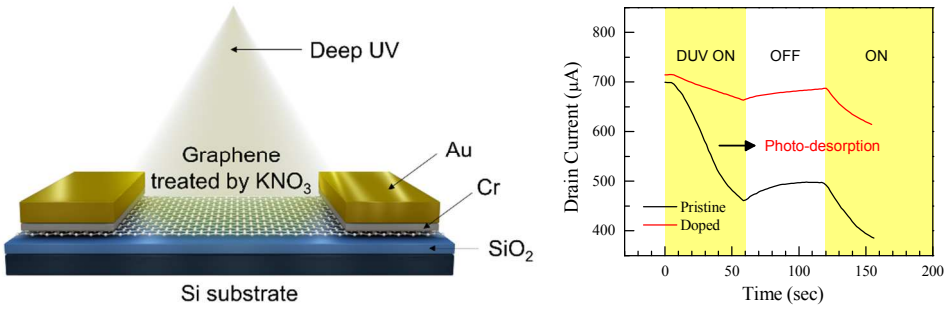

Stable and reversible doping of graphene by using KNO_3 solution and photo-desorption current response

M. Farooq Khan, M. Zahir Iqbal, M. Waqas Iqbal, Volodymyr M. Iermolenko, H. M. Waseem Khalil, Jungtae Nam, Keun Soo Kim, Hwayong Noh and Jonghwa Eom*

Department of Physics and Graphene Research Institute, Sejong University, Seoul 143-747, Korea

*E-mail: eom@sejong.ac.kr

Abstract

Graphene is easily p-doped by various impurities. Thus, finding a stable method of the n-doping of graphene is highly necessary for device fabrication. In this paper, the stable n-doping and charge carrier mobility improvement of chemical vapor deposition (CVD)-grown graphene by using KNO_3 solution were reported. Electron doping effect was examined by electrical transport measurement and Raman spectroscopy, and results suggested that the n-doping mechanism was due to ionic physisorption on graphene surface. The stable doping of graphene in atmospheric environment and at various temperatures (300, 50, 25, and 4.7 K) was also found. The n-doping effect was lifted and the charge neutrality point of doped graphene was restored to its initial state after annealing in Ar environment. Furthermore, the photo-desorption behavior of KNO_3-treated graphene under deep ultraviolet light was studied. Treatment by KNO_3 weakened the photo-desorption effect of CVD-grown graphene. This weakening effect was ascribed to the reduction of oxygen constituents on graphene surface, as further confirmed by X-ray photoelectron

spectroscopy. The chemical doping method using KNO_3 solution provided a novel route to the n-doping of graphene for the realization of high-performance graphene-based electronic devices.

1. Introduction

The interest on graphene, a single layer of sp^2-bonded carbon atoms, is due to its physical properties, such as ballistic charge transport, flexibility, thermal conductivity, and mechanical strength.[1-7] Importantly, the electron transport is described by the Dirac equation and this gives an access to quantum electrodynamics in a simple condensed matter experiment.[8] These superior properties make graphene a promising material for a wide range of nanoelectronics, photoelectronics, lithium ion batteries, and microelectronics.[9-12] Furthermore, tuning the characteristics of graphene, graphene oxides (GO) and reduced graphene oxides (rGO) are crucial in the production of electronic and organic photovoltaic devices.[9, 13-19] Although, doping can be done in many ways, such as metal decoration and ultra-violet (UV) light illumination to modulate the electrical properties of graphene; however, chemical doping is a simple approach to implement.[20-22] In fact, chemical doping is effective in manipulating the doping level of graphene and preserving its basic properties.[23] Surface charge transfer and substitutional doping can achieve chemical doping. Substitutional doping is a process of replacing carbon atoms in the lattice of graphene by heterogeneous atoms, such as nitrogen and boron.[24, 25] On one hand, substitutional doping may perturb the sp^2 hybridization of graphene. On the other hand, surface charge transfer doping would not disturb the structure of graphene and can be performed by adsorption of different chemical species, such as metals and organic molecules.[26-29] Surface charge transfer doping by chemical species or chemical ions do not damage the band structure of graphene.[23]

Recently, much attention has been widely focused on the photo-induced resistive responses of graphene and related materials. For example, ultrafast photodetectors were fabricated from graphene sheets. The generation and transport of photo-carriers were different

from conventional semiconductors.[30] The photo-response of graphene-based photodetectors has a vital role in optoelectronics. The photo-assisted desorption and re-adsorption of molecular species on graphene surface is the main dynamics for drain current variations under illumination.[31] In the range of visible to UV wavelength, the photo-induced desorption and re-adsorption result in variation of resistance in graphene film.[11, 32] Moreover, graphene is indeed a broadband saturable absorber that can function at both microwave and optical band. Saturable absorption and nonlinear phase shift may pave the way for graphene-based nonlinear photonics.[33, 34]

The electrical transport properties of graphene were reported to be very responsive to local perturbations and defects induced by adsorption of gas molecules, tuning the work function of graphene and graphene oxides using alkali metal carbonates, surface charge doping with various aromatic molecules, and chemical doping.[22, 27, 35-43] However, these reports were not focused on charge carrier mobility and stability of doping effect, which are easily changed by environmental factors, temperatures, and fabrication process, such as annealing. In addition, addressing the issues of photo-assisted response of graphene after chemical doping is required.

In this paper, back-gated field-effect transistor (FET) based on CVD-grown graphene was fabricated. An effective, air-stable chemical n-doping of CVD-grown graphene by using KNO_3 solution with improvement of charge carrier mobility was investigated. The maximum resistivity corresponding to the charge neutrality point was shifted towards negative voltage with increased KNO_3 treatment time. Raman spectroscopy and electrical transport measurements revealed the n-doping effect of CVD-grown graphene. The charge neutrality point of CVD-grown graphene was analyzed as a function of back-gate voltage. The doping effect of chemical solution can be erased after annealing the graphene, which reverted the charge neutrality point of graphene to its

position of pristine graphene. The photo-induced molecular desorption current of graphene, which can be modulated by chemical doping, was also studied. These electrical and photoelectrical measurement results of graphene showed that chemical doping by using KNO_3 solution is an effective and easily applicable approach for electronic and photo-electronic applications.

2. Experimental section

2.1 Synthesis of CVD-grown graphene

Large-area high-quality monolayer graphene was synthesized on thick Cu foils [Cu foil (LS Mtron 35 μm, LSU-STN)] by a thermal chemical vapor deposition system. The thermal CVD chamber was pumped with a pressure up to ~10^{-7} Torr. Then Cu substrate was heated to 1000 ºC in Ar gas with flow rate of 100 standard cubic centimeters per minute (sccm). In the subsequent process, H_2 gas was introduced into the chamber at 50 sccm for 20 min and CH_4 gas was flown at 10 sccm. The flow rate of H_2 gas was then gradually reduced to 10 sccm. After the growth of graphene, the Cu foil was cooled down to room temperature. The graphene films on Cu foil were transferred on a Si substrate by wet transfer method. The Cu foil was spin coated with a thin layer of polymethyl methacrylate (PMMA) and etched away in a 1 M solution of ammonium persulfate [APS, $(NH_4)_2S_2O_8$], and the graphene on PMMA membrane was rinsed with de-ionized water. Then the graphene on the PMMA membrane was transferred to a degenerately p-doped Si substrate with a 300 nm-thick SiO_2 and soaked in acetone for 24 hours to dissolve the PMMA layer.[44]

2.2 Raman characterization and device fabrication

Raman spectra were measured using a Renishaw micro-spectrometer with a laser wavelength of 514 nm at room temperature. The spot size was ~1 μm and the power was maintained at ~1.0 mW to reduce the heating effects. The big patterns were first made of Cr/Au (5/30 nm) films using photolithography and metals were deposited by thermal evaporation system. The final contacts to graphene were made of Cr/Au (10/60 nm) by using e-beam lithography and thermal evaporation. All devices in our experiment have same dimensions as shown in Figure 1a. The length and width of devices were ~10 μm and ~5 μm, respectively. The four-terminal method was employed for electrical measurements using a standard lock-in technique. Samples were in vacuum during the electrical measurement. The tuning of graphene properties by KNO_3 was investigated by electrical transport measurements and Raman spectroscopy. Electrical measurement and Raman spectroscopy were performed on the same devices before and after different treatment times of KNO_3. The chemical compound KNO_3 is an ionic salt of potassium ions K^+ and nitrate ions NO_3^-, which was dissolved in de-ionized water to make the concentration of 0.1 M solution. The samples were dipped for specific time in the KNO_3 solution and then placed on a hot plate to dry at 100 ºC for 2 min. The deep ultraviolet (DUV) light (λ = 220 nm and average intensity of 11 $mWcm^{-2}$) was used for the photo-response measurement.

3. Results and discussion

3.1 Raman characterization

The optical image of FET based on CVD-grown monolayer graphene is shown in Figure 1a. The graphene channel was further examined by scanning electron microscopy (SEM) image as shown in Figure S1c (Supporting Information). The quality of pristine and chemically treated graphene was analyzed by Raman spectroscopy at ambient environment. Raman spectroscopy is a rapid

tool to characterize and identify the number of graphene layers. The Figure 2a shows the Raman spectra of pristine and sequentially doped graphene (Device-1). The G peak corresponds to the E_{2g} optical phonon at the Brillouin zone center. The second order of the D peak is the 2D peak, which originates from a scattering process where momentum conservation is fulfilled by two phonons with opposite wave vectors.[45, 46] The characteristic G and 2D peaks for pristine graphene appeared around 1587 and 2685 cm^{-1}, respectively. The intensity ratio of 2D and G peaks was ~4, which was greater than 2, confirming the signature of monolayer graphene as reported in previous publications.[47-50] In Figure 2a, the shift of G and 2D peaks can be clearly observed after KNO_3 treatments. The absence of D peak, seen in the shaded rectangle box of Figure 2a, demonstrated the defect- free doping of graphene by KNO_3 solution, suggesting that KNO_3 solution did not alter the basic structure of monolayer graphene. The shifts of G and 2D peaks increased with increased treatment time. The G peak was shifted from 1587 to 1580 cm^{-1}, and the 2D peak moved from 2685 to 2680 cm^{-1}. Figure 2b sequentially marked the positions of G and 2D peaks for different treatment time. The downshift of G and 2D peak positions was attributed to the n-doping of graphene. The down and upward shifts of G and 2D peak positions could be attributed to n-type and p-type doping of graphene, respectively.[21, 35, 40, 51-54] Figure 2c shows the intensity ratio of 2D and G peak (I_{2D}/I_G) before and after KNO_3 treatment for different times. The I_{2D}/I_G decreased with increased treatment time for monolayer graphene, where the reduction of I_{2D}/I_G indicated the doping effect on graphene.[26, 55, 56] Figure 2d shows full width half maximum (FWHM) of 2D band for monolayer graphene before and after KNO_3 treatments. The FWHM decreased with increased treatment time by KNO_3 solution, which signified the screening of impurity scatterings.[57] The stiffness of 2D peak as a function of treatment time is shown in Figure S2 (Supporting Information).

3.2 Electrical transport property

The influences of electron doping on FET based on CVD-grown monolayer graphene (Device-1) were also observed by electrical transport measurements. The resistivity as a function of gate voltage (V_g) before and after KNO_3 treatments of monolayer graphene for different time is shown in Figure 3a. The charge neutrality point (V_{CNP}) of pristine monolayer graphene (Device-1) was observed at +49 V and then shifted towards +6 V after 1 min treatment time. The shift progressively increased with increased treatment time and V_{CNP} saturated almost at -29 V after 20 min treatment. Similarly, the electrical properties of another FET based on CVD-grown monolayer graphene (Device-2) were measured and showed similar trend as Device-1. The V_{Dirac} of Device-2 was observed at +17 V and then shifted towards -2V after 1 min treatment time. The shift gradually increased with increased treatment time and V_{CNP} saturated at -26 V after 20 min treatment, as shown in Figure 3b. The shift of V_{CNP} as a function of treatment time for graphene samples (Device-1 and -2) is shown in Figure 3c.

The saturation of charge neutrality point depended on the adsorption limit of K^+ ions on graphene surface, which may combined with oxygen atom/molecules. The transition of charge neutrality point towards negative gate voltage was a clear indication of the n-doping effect. The change in charge carrier density (Δn) in Device-1 and -2 as a function of KNO_3 treatment time is shown in Figure S3 (Supporting Information) and it clearly shows that charge carrier density notably changed after different KNO_3 treatment time. The change in Δn is related to the tuning of the Fermi level in the graphene layer from valence to conduction band. The change in charge carrier density (Δn) of graphene layers were calculated by using the relation $\Delta n = C_g(V_g - V_{CNP})/e$, where C_g is the gate capacitance ~115 aF/ μm^2 for our Si/SiO_2 substrate, V_{CNP} is the

charge neutrality point of graphene samples, V_g is the back gate voltage, and *e* is the electric charge. Figure 3d shows the electron and hole mobility of Device-1 and -2 as a function of treatment time. The field effect mobilities of the different graphene samples were obtained using relation $\mu = (1/C_g)\ (\partial\sigma/\partial V_g)$, where $\sigma = 1/\rho$ is the conductivity of samples. The mobility of pristine and doped graphene was calculated based on $(\partial\sigma/\partial V_g)$, fitted to the linear region of their respective conductivity data. The charge carrier mobility of graphene samples improved with increased treatment time. The hole and electron mobility of Device-1 were 695 and 226 $cm^2V^{-1}s^{-1}$ in pristine state and improved gradually with increase of treatment time and reached to 1416 and 1581 $cm^2V^{-1}s^{-1}$ after 20 min doping, respectively. For Device-2 the hole and electron mobility were around 3658 and 2433 $cm^2V^{-1}s^{-1}$ in pristine state. The hole and electron mobility were enhanced progressively with increase of doping time and they reached to 5157 and 5510 $cm^2V^{-1}s^{-1}$ after 20 min doping, respectively. The electron mobility of Device-1 was enhanced more than five times, which was a promising result. The doping treatments of graphene mostly showed degradation of mobility.[35, 52, 58, 59] The mobility improvement may be due to the ionic screening of charged-impurities scattering.[23, 60] These results suggested that the performance of graphene devices was improved by chemical doping of KNO_3 solution. Theoretical investigations showed that the K^+ ions preferably reside in hollow site of graphene honeycomb structure and transfer electrons to graphene.[61, 62] The adsorption of K^+ ions was further confirmed by X-ray photoelectron spectroscopy of the CVD-grown graphene treated by KNO_3 solution for 20 min. In Figure S4 (Supporting Information) a peak was observed at ~295 eV, which correspond to the potassium related peak confirming the adsorption of K^+ ion on the surface of graphene.

3.3 Stability of doping at low temperature

At different temperatures (300, 50, 25, and 4.7 K), the resistivity as a function of V_g before and after KNO_3 treatment of monolayer CVD-grown graphene FET (Device-3) are shown in Figures 4a and 4b, respectively. The investigation of pristine monolayer graphene FET (Device-3) at different temperatures (300, 50, 25, and 4.7 K) shows that V_{CNP} remains stable at similar value. The V_{CNP} of pristine graphene was near +10 V at 300 K and remained at similar value at different low temperatures. Afterward, the same graphene sample (Device-3) was doped for 20 min by KNO_3 solution. V_{CNP} moved towards negative gate voltage around -10 V at 300 K owing to the n-doping effect. The V_{CNP} of doped graphene remains stable at similar value around -10 V at different low temperatures (50, 25, and 4.7 K). No effect of temperatures was seen on the V_{CNP} of pristine and doped graphene and V_{CNP} remains stable, as shown in Figures 4a and 4b, respectively. The charge carriers mobility of pristine and doped graphene samples (Device-3) at different low temperatures were measured, as shown in Figures 4c and 4d, respectively. The electron and hole mobility of pristine graphene at 300 K were about 1650 and 4090 cm^2/Vs and gradually increased to 3900 and 5750 cm^2/Vs at 4.7 K, respectively. The electron and hole mobility of graphene after 20 min KNO_3 treatment were about 2950 and 4870 cm^2/Vs at 300 K and increased to 6610 and 6160 cm^2/Vs at 4.7 K, respectively.

3.4 Stability of doping in atmospheric environment and annealing effect

The stability of doped graphene in atmospheric environment and the annealing effect in Ar gas flow were examined. Figure 5a shows resistivity as a function of back gate voltage for the graphene FET (Device-4), where V_{CNP} in pristine state was observed at +63 V. After KNO_3 doping treatment for 20 min, V_{CNP} shifted towards -20 V. Interestingly, V_{CNP} in atmospheric

environment remained the same even after 2 months, as shown in Figure 5a. However, V_{CNP} after annealing at 200 ºC in Ar environment for two hours restored V_{CNP} to +65 V, which was very close to V_{CNP} in the pristine state. The same phenomenon was observed for other graphene FETs. This result might be ascribed to the decomposition of potassium oxide compounds when annealed in Ar environment. Table 1 in Supporting Information shows the charge carrier mobility of pristine, doped, after 2 months in air, and annealed graphene sample (Device-4). Interestingly, the carrier mobility of doped graphene remained almost the same after 2 months, but after annealing the hole and electron, its mobility was reduced to the values comparable to the pristine state. In addition, Raman spectra were examined in each state, as shown in Figure 5b. After KNO_3 chemical doping, the downward shift remained almost the same after 2 months. However, the upward shift was observed after annealing in Ar gas flow as shown in Figure 5b. After annealing, a small D peak around 1350 cm^{-1} was found owing to increased disorder or slight structural deformation after annealing.[63] Figure 5c elaborates the G and 2D peak positions of Raman spectrum at each step. When Device-4 was annealed for two hours at 200 ºC in Ar gas flow, the Raman spectrum showed a decrease in 2D peak intensity and up-shift in the positions of G and 2D peaks, which were related to the decomposition of potassium oxide compounds from graphene surface.

3.4 DUV photocurrent response

The photo-desorption induced current of pristine and KNO_3 treated (20 min) CVD-grown monolayer graphene sample (Device-5) was studied. The KNO_3 doping was confirmed by checking the resistivity as a function of V_g before and after treatments, as shown in Figure 6b. The schematic of photocurrent measurement is shown in Figure 1b. The photocurrent of

graphene decreases with DUV light exposure because number of charge carriers is reduced as gas molecules adsorbed at defect sites are partially removed by DUV light. It is well known that CVD-grown graphene acquires more dangling bond and vacancies during growth as compared to mechanically exfoliated graphene. The dangling bonds and vacancies contribute to the increase of defect sites, which play vital role in photo-desorption current.[5, 64, 65] We further investigated the effect of KNO_3 treatment on photo-desorption current of CVD-grown graphene. Under DUV light illumination, the photo-desorption current (ΔI_p) of pristine graphene was ~239 μA, which corresponds to 34% of reduction in drain current, in the first 60s; however, ΔI_p of doped graphene by KNO_3 solution was reduced to ~51 μA, which corresponds to 7.2% of reduction in drain current, as shown in Figure 6a. The photo-desorption current became less significant after KNO_3 doping because this decrease in photo-desorption current was attributed to the passivation of the oxygen-bearing functionalities in CVD-grown graphene by KNO_3 solution.[11, 36] The reduction of oxygen species from graphene was verified by X-ray photoelectron spectroscopy (XPS). In Figure 6c, the C 1s peak of pristine graphene can be analyzed through the three components arising from C-C (284.6 eV), C-O (285.4 eV), and C=O (288.6 eV). The intensities of carbon atom bond to oxygen were significantly reduced after doping in KNO_3 solution for 20 min, as shown in Figure 6d.[66]

4. Conclusions

An efficient method of doping CVD-grown graphene was investigated, and an effective chemical solution for doping without disturbing the basic structure of graphene FET devices was proposed. The shift in the G and 2D bands in the Raman spectra towards lower wavenumber was attributed to n-doping in the graphene devices. In the back-gate-voltage dependent resistivity

measurement the charge neutrality point shifted toward a more negative gate voltage with increased chemical treatment time that accompanied the mobility improvement of charge carriers. The mechanism of n-doping was suggested to be electrostatic doping by ionic physisorption of potassium ions on the graphene surface. The doping effect was air-stable in graphene devices and also at different temperatures from 300 K to 4.7 K. More importantly, the charge neutrality point of doped graphene was restored to initial position of pristine graphene after annealing at 200 ºC for two hours in Ar environment. The photo-desorption current in graphene was investigated under DUV light. The photo-desorption current became less significant after KNO_3 treatment. The XPS analysis indicated that the KNO_3 treatment deoxygenated the graphene. The effective control of charge carriers in graphene with stability and reversibility of the doping effect is a rewarding approach in graphene based electronic applications.

Acknowledgment

This research was supported by Nano-Material Technology Development Program (2012M3A7B4049888) through the National Research Foundation of Korea (NRF) funded by the Ministry of Science, ICT and Future Planning. This research was also supported by Priority Research Center Program (2010-0020207) and the Basic Science Research Program (2013R1A1A2061396) through NRF funded by the Ministry of Education.

References

1. F. Schedin, A. K. Geim, S. V. Morozov, E. W. Hill, P. Blake, M. I. Katsnelson and K. S. Novoselov, *Nat Mater*, 2007, **6**, 652-655.
2. S. V. Morozov, K. S. Novoselov, M. I. Katsnelson, F. Schedin, D. C. Elias, J. A. Jaszczak and A. K. Geim, *Phys Rev Lett*, 2008, **100**.
3. A. K. Geim, *Science*, 2009, **324**, 1530-1534.
4. J. H. Chen, C. Jang, S. D. Xiao, M. Ishigami and M. S. Fuhrer, *Nat Nanotechnol*, 2008, **3**, 206-209.
5. K. S. Kim, Y. Zhao, H. Jang, S. Y. Lee, J. M. Kim, K. S. Kim, J. H. Ahn, P. Kim, J. Y. Choi and B. H. Hong, *Nature*, 2009, **457**, 706-710.
6. M. Y. Han, B. Ozyilmaz, Y. B. Zhang and P. Kim, *Phys Rev Lett*, 2007, **98**.
7. G. Viskadouros, D. Konios, E. Kymakis and E. Stratakis, *Appl Phys Lett*, 2014, **105**.
8. K. S. Novoselov, A. K. Geim, S. V. Morozov, D. Jiang, M. I. Katsnelson, I. V. Grigorieva, S. V. Dubonos and A. A. Firsov, *Nature*, 2005, **438**, 197-200.
9. F. Schwierz, *Nat Nanotechnol*, 2010, **5**, 487-496.
10. D. S. Hecht, L. B. Hu and G. Irvin, *Adv Mater*, 2011, **23**, 1482-1513.
11. Y. M. Shi, W. J. Fang, K. K. Zhang, W. J. Zhang and L. J. Li, *Small*, 2009, **5**, 2005-2011.
12. J. Hassoun, F. Bonaccorso, M. Agostini, M. Angelucci, M. G. Betti, R. Cingolani, M. Gemmi, C. Mariani, S. Panero, V. Pellegrini and B. Scrosati, *Nano Lett*, 2014, **14**, 4901-4906.
13. M. Kim, N. S. Safron, E. Han, M. S. Arnold and P. Gopalan, *Nano Lett*, 2010, **10**, 1125-1131.
14. J. W. Bai and Y. Huang, *Mat Sci Eng R*, 2010, **70**, 341-353.
15. N. S. Safron, A. S. Brewer and M. S. Arnold, *Small*, 2011, **7**, 492-498.
16. D. Konios, C. Petridis, G. Kakavelakis, M. Sygletou, K. Savva, E. Stratakis and E. Kymakis, *Advanced Functional Materials*, 2015, **25**, 2213-2221.
17. E. Stratakis, K. Savva, D. Konios, C. Petridis and E. Kymakis, *Nanoscale*, 2014, **6**, 6925-6931.

18. L. Sun and B. Fugetsu, *Materials Letters*, 2013, **109**, 207-210.

19. D. Konios, M. M. Stylianakis, E. Stratakis and E. Kymakis, *J Colloid Interf Sci*, 2014, **430**, 108-112.

20. H. T. Liu, Y. Q. Liu and D. B. Zhu, *J Mater Chem*, 2011, **21**, 3335-3345.

21. M. Z. Iqbal, S. Siddique, M. W. Iqbal and J. Eom, *J Mater Chem C*, 2013, **1**, 3078-3083.

22. M. W. Iqbal, A. K. Singh, M. Z. Iqbal and J. Eom, *J Phys-Condens Mat*, 2012, **24**.

23. M. F. Khan, M. Z. Iqbal, M. W. Iqbal and J. Eom, *Science and Technology of Advanced Materials*, 2014, **15**, 055004.

24. B. D. Guo, Q. A. Liu, E. D. Chen, H. W. Zhu, L. A. Fang and J. R. Gong, *Nano Lett*, 2010, **10**, 4975-4980.

25. D. C. Wei, Y. Q. Liu, Y. Wang, H. L. Zhang, L. P. Huang and G. Yu, *Nano Lett*, 2009, **9**, 1752-1758.

26. J. Lee, K. S. Novoselov and H. S. Shin, *Acs Nano*, 2011, **5**, 608-612.

27. X. C. Dong, D. L. Fu, W. J. Fang, Y. M. Shi, P. Chen and L. J. Li, *Small*, 2009, **5**, 1422-1426.

28. W. Chen, S. Chen, D. C. Qi, X. Y. Gao and A. T. S. Wee, *J Am Chem Soc*, 2007, **129**, 10418-10422.

29. R. Voggu, B. Das, C. S. Rout and C. N. R. Rao, *J Phys-Condens Mat*, 2008, **20**.

30. F. N. Xia, T. Mueller, Y. M. Lin, A. Valdes-Garcia and P. Avouris, *Nat Nanotechnol*, 2009, **4**, 839-843.

31. C. G. Kang, S. K. Lee, S. H. Choe, Y. G. Lee, C. L. Lee and B. H. Lee, *Opt Express*, 2013, **21**, 23391-23400.

32. P. Z. Sun, M. Zhu, K. L. Wang, M. L. Zhong, J. Q. Wei, D. H. Wu, Y. Cheng and H. W. Zhu, *Appl Phys Lett*, 2012, **101**.

33. Z. W. Zheng, C. J. Zhao, S. B. Lu, Y. Chen, Y. Li, H. Zhang and S. C. Wen, *Opt Express*, 2012, **20**, 23201-23214.

34. H. Zhang, S. Virally, Q. L. Bao, L. K. Ping, S. Massar, N. Godbout and P. Kockaert, *Opt Lett*, 2012, **37**, 1856-1858.

35. A. K. Singh, M. W. Iqbal, V. K. Singh, M. Z. Iqbal, J. H. Lee, S. H. Chun, K. Shin and J. Eom, *J Mater Chem*, 2012, **22**, 15168-15174.

36. J. Lin, J. B. Zhong, J. R. Kyle, M. Penchev, M. Ozkan and C. S. Ozkan, *Nanotechnology*, 2011, **22**.

37. T. O. Wehling, K. S. Novoselov, S. V. Morozov, E. E. Vdovin, M. I. Katsnelson, A. K. Geim and A. I. Lichtenstein, *Nano Lett*, 2008, **8**, 173-177.

38. Y. Chen, B. Gao, J. X. Zhao, Q. H. Cai and H. G. Fu, *J Mol Model*, 2012, **18**, 2043-2054.

39. M. Z. Iqbal, A. K. Singh, M. W. Iqbal, S. Seo and J. Eom, *J Appl Phys*, 2012, **111**.

40. M. Iqbal, O. Kelekci, M. Iqbal and J. Eom, *Carbon*, 2013, **59**, 366-371.

41. Z. Zhang, H. Huang, X. Yang and L. Zang, *The Journal of Physical Chemistry Letters*, 2011, **2**, 2897-2905.

42. K. C. Kwon, K. S. Choi, B. J. Kim, J. L. Lee and S. Y. Kim, *J Phys Chem C*, 2012, **116**, 26586-26591.

43. G. Kakavelakis, D. Konios, E. Stratakis and E. Kymakis, *Chem Mater*, 2014, **26**, 5988-5993.

44. K. S. Kim, Y. Zhao, H. Jang, S. Y. Lee, J. M. Kim, K. S. Kim, J.-H. Ahn, P. Kim, J.-Y. Choi and B. H. Hong, *Nature*, 2009, **457**, 706-710.

45. A. Ferrari and J. Robertson, *Phys Rev B*, 2000, **61**, 14095.

46. A. C. Ferrari, J. C. Meyer, V. Scardaci, C. Casiraghi, M. Lazzeri, F. Mauri, S. Piscanec, D. Jiang, K. S. Novoselov, S. Roth and A. K. Geim, *Phys Rev Lett*, 2006, **97**.

47. X. Li, W. Cai, J. An, S. Kim, J. Nah, D. Yang, R. Piner, A. Velamakanni, I. Jung and E. Tutuc, *Science*, 2009, **324**, 1312-1314.

48. A. Ferrari, J. Meyer, V. Scardaci, C. Casiraghi, M. Lazzeri, F. Mauri, S. Piscanec, D. Jiang, K. Novoselov and S. Roth, *Phys Rev Lett*, 2006, **97**, 187401.

49. Z. Ni, H. Wang, J. Kasim, H. Fan, T. Yu, Y. Wu, Y. Feng and Z. Shen, *Nano Lett*, 2007, **7**, 2758-2763.

50. D. Yoon, Y.-W. Son and H. Cheong, *Phys Rev Lett*, 2011, **106**, 155502.

51. H. J. Shin, W. M. Choi, D. Choi, G. H. Han, S. M. Yoon, H. K. Park, S. W. Kim, Y. W. Jin, S. Y. Lee, J. M. Kim, J. Y. Choi and Y. H. Lee, *J Am Chem Soc*, 2010, **132**, 15603-15609.

52. A. K. Singh, M. Ahmad, V. K. Singh, K. Shin, Y. Seo and J. Eom, *Acs Appl Mater Inter*, 2013, **5**, 5276-5281.

53. K. K. Kim, A. Reina, Y. M. Shi, H. Park, L. J. Li, Y. H. Lee and J. Kong, *Nanotechnology*, 2010, **21**.

54. S. Tongay, K. Berke, M. Lemaitre, Z. Nasrollahi, D. B. Tanner, A. F. Hebard and B. R. Appleton, *Nanotechnology*, 2011, **22**.

55. A. Das, S. Pisana, B. Chakraborty, S. Piscanec, S. K. Saha, U. V. Waghmare, K. S. Novoselov, H. R. Krishnamurthy, A. K. Geim, A. C. Ferrari and A. K. Sood, *Nat Nanotechnol*, 2008, **3**, 210-215.

56. K. C. Kwon, K. S. Choi, C. Kim and S. Y. Kim, *physica status solidi (a)*, 2014.

57. Z. H. Ni, T. Yu, Z. Q. Luo, Y. Y. Wang, L. Liu, C. P. Wong, J. M. Miao, W. Huang and Z. X. Shen, *Acs Nano*, 2009, **3**, 569-574.

58. Y. Kim, J. Ryu, M. Park, E. S. Kim, J. M. Yoo, J. Park, J. H. Kang and B. H. Hong, *Acs Nano*, 2014, **8**, 868-874.

59. W. H. Lee, J. W. Suk, J. Lee, Y. F. Hao, J. Park, J. W. Yang, H. W. Ha, S. Murali, H. Chou, D. Akinwande, K. S. Kim and R. S. Ruoff, *Acs Nano*, 2012, **6**, 1284-1290.

60. F. Chen, J. L. Xia and N. J. Tao, *Nano Lett*, 2009, **9**, 1621-1625.

61. O. Faye, *The African Review of Physics*, 2012, **7**.

62. B. Oli, C. Bhattarai, B. Nepal and N. Adhikari, in *Advanced Nanomaterials and Nanotechnology*, Springer, 2013, pp. 515-529.

63. C.-S. Park, Y. Zhao, H. Kim, Y. Shon and E. K. Kim, *Chem Commun*, 2014.

64. H. E. Romero, P. Joshi, A. K. Gupta, H. R. Gutierrez, M. W. Cole, S. A. Tadigadapa and P. C. Eklund, *Nanotechnology*, 2009, **20**.

65. C. Rusu and J. Yates, *Langmuir*, 1997, **13**, 4311-4316.

66. Z. B. Lei, L. Lu and X. S. Zhao, *Energ Environ Sci*, 2012, **5**, 6391-6399.

Figure captions

Figure 1. (a) Optical photo of CVD-grown graphene FET device. (b) Schematic of CVD-grown graphene FET under DUV light.

Figure 2. Raman spectra of (a) pristine and doped CVD-grown graphene (Device-1) for different times. The rectangle green box represents the absence of D peak. (b) Position of G (blue) and 2D (green) peaks as a function of treatment time. (c) Ratio of intensities for 2D and G peaks is plotted as a function of treatment time. (d) Full width at half-maximum of 2D band of Raman spectra with respect to treatment time.

Figure 3. Resistivity as a function of V_g for (a) (Device-1) and (b) (Device-2) of CVD-grown graphene before and after KNO_3 treatment for different times. (c) Shift of charge neutrality point positions of (Device-1 and -2) as a function of treatment time. (d) Electron (solid circles) and hole (open circles) mobilities of (Device-1 and -2) as a function treatment time.

Figure 4. Resistivity as a function of V_g for (a) undoped and (b) doped (20 min) CVD-grown graphene (Device-3) at different low temperatures. The electron and hole mobilities of undoped (c) and doped (d) CVD-grown graphene as a function of temperature.

Figure 5. (a) Resistivity as a function of V_g for pristine, doped (20 min), after 2 months, and annealed CVD-grown graphene (Device-4). (b) Raman spectra of pristine, doped (20 min), after

2 months, and annealed graphene (Device-4). (c) Peak (G and 2D) positions of pristine, doped (20 min), after 2 months, and annealed graphene (Device-4).

Figure 6. (a) Drain current of pristine and doped (for 20 min) CVD-grown graphene (Device-5) as a function of time under DUV illumination in a vacuum at (V_{ds} = 1 V and V_g = 0 V). (b) Charge neutrality points of pristine and doped (for 20 min) graphene (Device-5). C 1s XPS spectra of (c) pristine and (d) doped CVD-grown graphene.

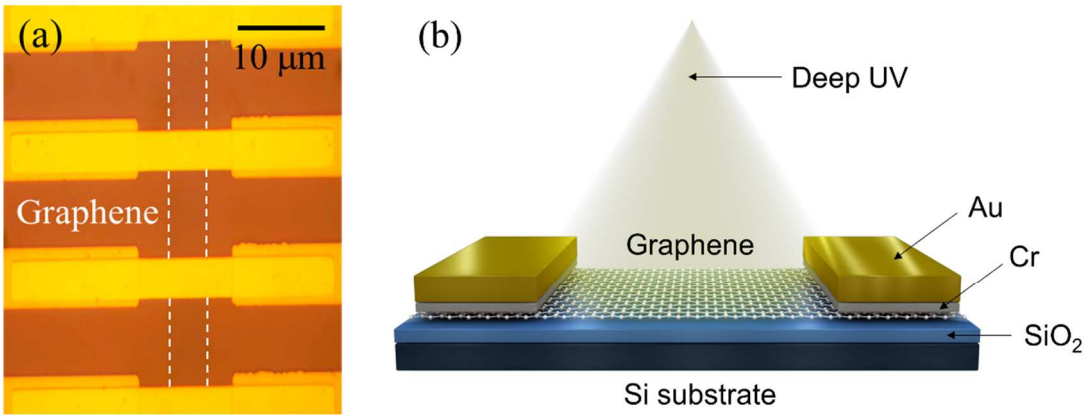

Figure 1

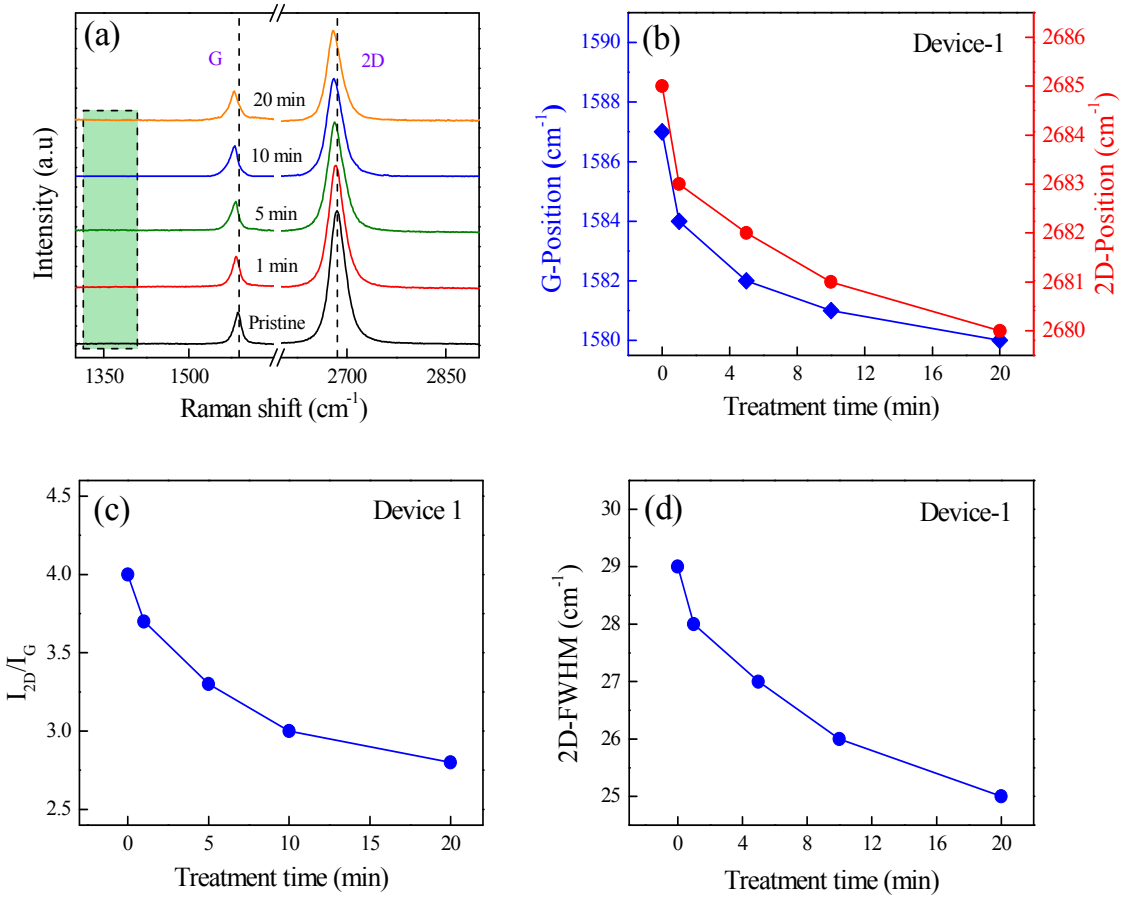

Figure 2

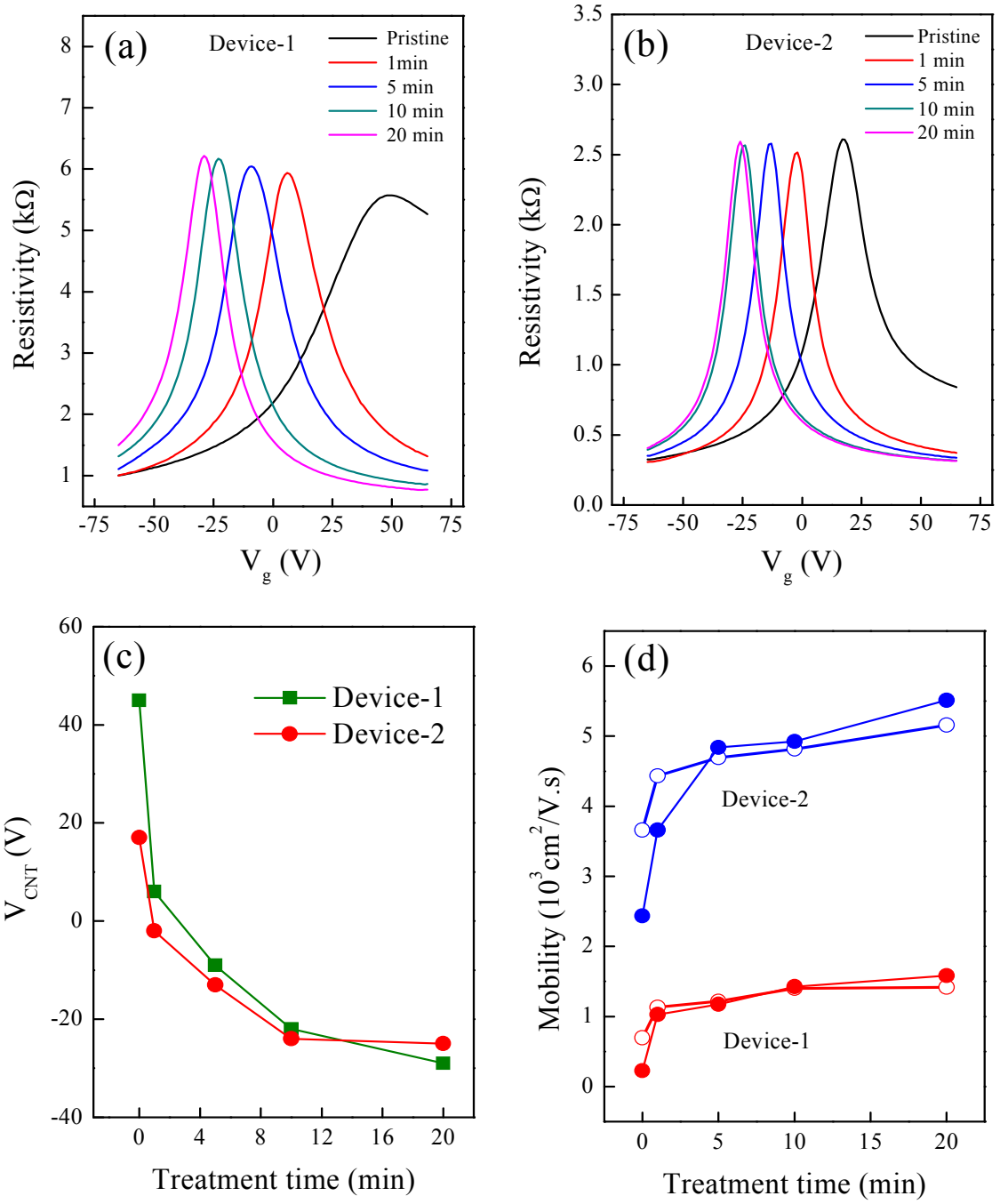

Figure 3

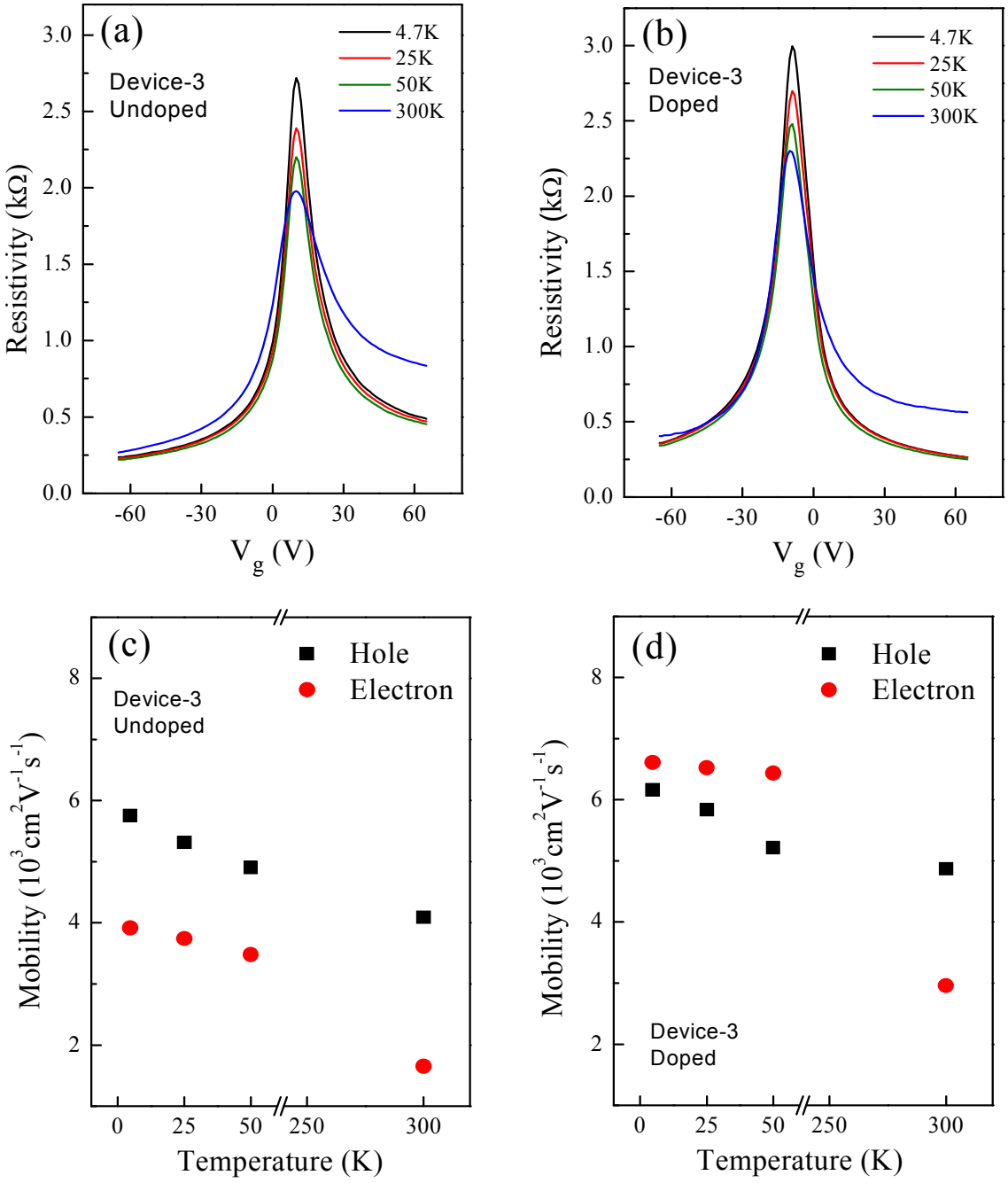

Figure 4

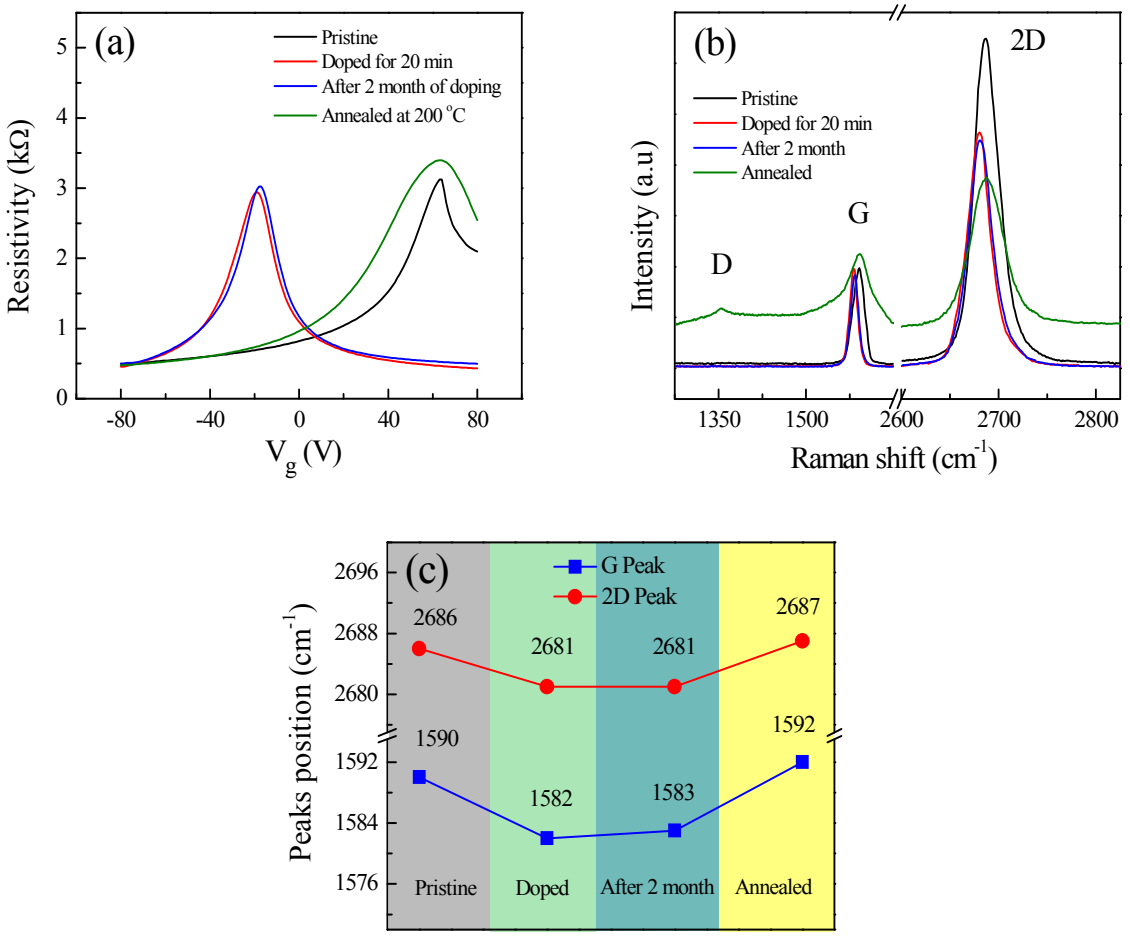

Figure 5

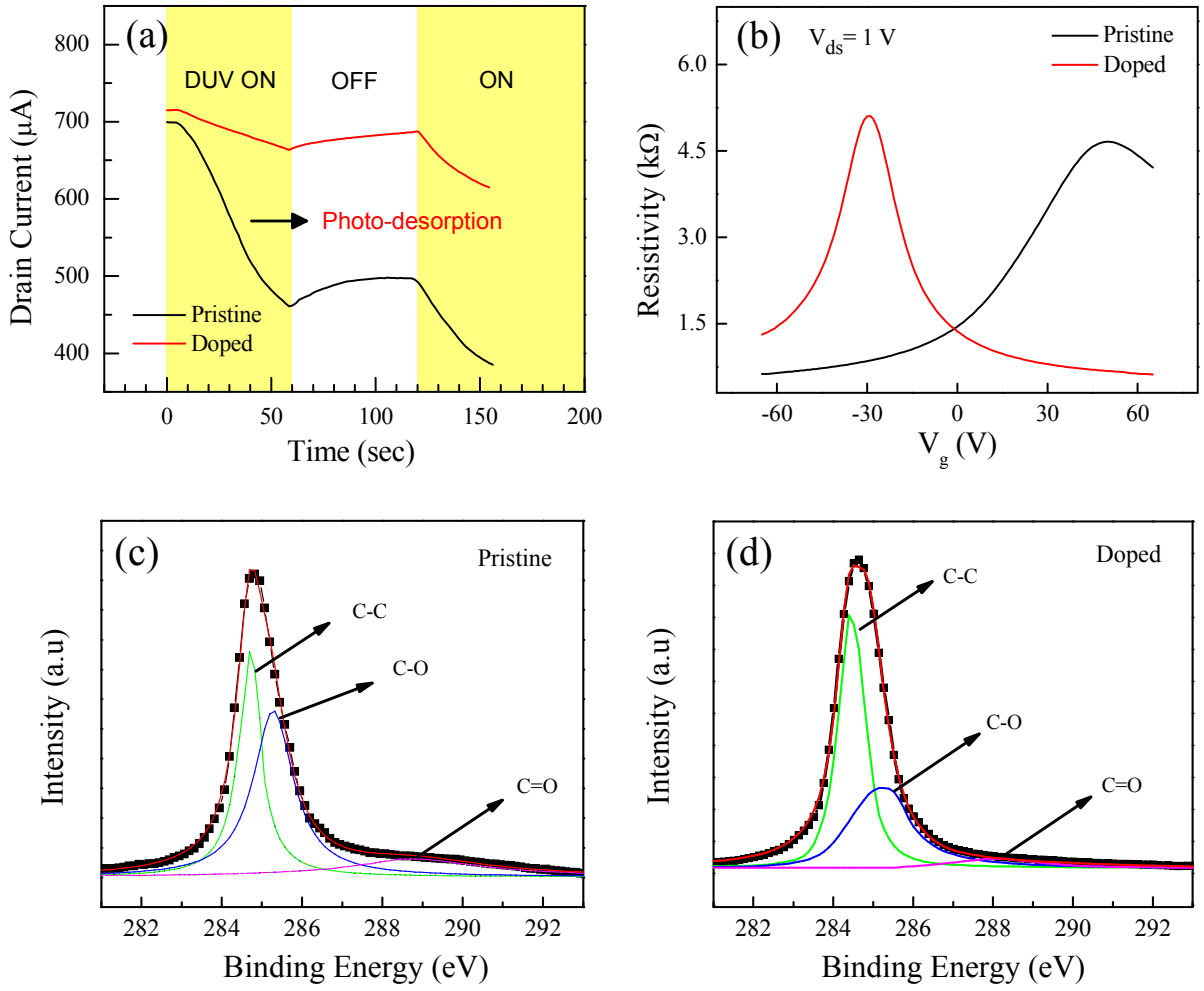

Figure 6